Elastomers and Composites
Vol. 59, No. 1, pp. 1~7 (March 2024)

Print ISSN 2092-9676/Online ISSN 2288-7725
DOI: https://doi.org/10.7473/EC.2024.59.1.1

# Synthesis of Nanorod g-$C_3N_4$/$Ag_3PO_4$ Composites and Photocatalytic Activity for Removing Organic Dyes under Visible Light Condition

**Se Hwan Park*, Jeong Won Ko**, and Weon Bae Ko*,***,†**

*Department of Convergence Science, Graduate School, Sahmyook University, Seoul 01795, Republic of Korea
**Department of Animal Resources Science, Sahmyook University, Seoul 01795, Republic of Korea
***Department of Chemistry, Sahmyook University, Seoul 01795, Republic of Korea

(Received January 9, 2024, Revised February 14, 2024, Accepted February 21, 2024)

**Abstract:** Nanorod graphitic carbon nitride (g-$C_3N_4$) was synthesized by reacting melamine ($C_3H_6N_6$) with trithiocyanuric acid ($C_3H_3N_3S_3$) in distilled water for 10 h at room temperature. The resulting mixture was calcined at 550°C for 2 h in an electric furnace under an air atmosphere. Nanorod g-$C_3N_4$/$Ag_3PO_4$ composites were prepared by adding nanorod graphitic carbon nitride (g-$C_3N_4$) powder, silver nitrate ($AgNO_3$), ammonia ($NH_3 \cdot H_2O$, 25.0-30.0%), and sodium hydrogen phosphate ($Na_2HPO_4$) to distilled water. The samples were characterized via X-ray diffraction, scanning electron microscopy, and Fourier-transform infrared spectroscopy. The photocatalytic activities of the nanorod g-$C_3N_4$/$Ag_3PO_4$ composites were demonstrated via the degradation of organic dyes, such as methylene blue and methyl orange, under blue light-emitting diode irradiation and evaluated using UV-vis spectrophotometry.

**Keywords:** Nanorod g-$C_3N_4$, $Ag_3PO_4$, photocatalytic activities, organic dyes, blue LED

## Introduction

Wastewater from the textile industry contains large amounts of dyes that can be harmful to the environment.[1,2] Dyes are a significant water pollutant in the wastewater of textile, leather, food processing, dyeing, cosmetics, paper, and dye manufacturing industries.[3,4] Fortunately, the problem of water pollution from dyes has been solved with semiconductor photocatalytic technology.[5-7] The degradation of organic pollutants using photocatalysis is a very promising method that accessed as an economical and environmentally friendly solution.[8,9] Among the photocatalysts, titanium oxide ($TiO_2$)-based nanomaterials are considered among the most reliable photocatalytic materials for degrading toxic and hazardous organic pollutants.[10,11] However, $TiO_2$ is only responsive to wavelengths in the ultraviolet light, which can absorb only 4% of the solar spectrum.[12] Therefore, there is need to enhance the photocatalyst capability to absorb solar energy.[13,14]

Among semiconductor photocatalysts, graphite-like carbon nitride has attracted huge attention due to its unique properties, such as high chemical stability, high thermal and photochemical stability, strong mechanical properties, and nontoxicity.[15,16] Graphitic carbon nitride forms a 2D layer derived from the tri-s-triazine unit structures of carbon and nitrogen. These 2D layers are stacked together by strong van der Waals forces.[17,18]

Since the discovery by Wang's group in 2009, metal-free graphite nitride (g-$C_3N_4$) has received considerable attention from scientists.[19] The g-$C_3N_4$ has been reported as a metal-free polymer-like semiconductor photocatalyst with thermal and chemical stability as well as low cost.[20] The g-$C_3N_4$ photocatalyst has a bandgap of 2.7 eV and can absorb light up to 450 nm.[21] However, the application of single g-$C_3N_4$ photocatalyst has been limited by high electron-hole recombination and low specific surface area.[22] To overcome the limitation of photocatalyst, several strategies, such as combinations with metals and non-metals and heterojunction configurations, have been used for g-$C_3N_4$.[23,24]

$Ag_3PO_4$ photocatalyst has received great attention owing to its bandgap (2.45 eV) and excellent visible light-driven photocatalytic activity for the degradation of organic pollutants.[25,26] $Ag_3PO_4$ contains an electric field between the $PO_4^{3-}$ and $Ag^+$ ions, resulting in a quantum efficiency of approximately 90% at 400-480 nm due to the separation of the

†Corresponding author E-mail: kowb@syu.ac.kr

photoelectron-hole pairs.[27,28]

In this study, the photocatalytic activities of the nanorod g-$C_3N_4$/$Ag_3PO_4$ were investigated to remove organic dyes, such as MB and MO, under blue LED (at 450 nm).

## Experimental

### 1. Materials

Melamine ($C_3H_6N_6$), sodium hydrogen phosphate ($Na_2HPO_4$) and trithiocyanuric acid ($C_3H_3N_3S_3$) were purchased from Alfa Aesar. Ammonia solution ($NH_3{\cdot}H_2O$ 25.0%~30.0%), ethyl alcohol ($C_2H_5OH$ 99.9%), methylene blue (MB), methyl orange (MO) and silver nitrate ($AgNO_3$) were purchased from Samchun Chemicals.

### 2. Instruments

XRD pattern and crystallite size of the synthesized samples were obtained using X-ray diffraction (Bruker, D8 Advance) with a Cu Kα radiation source (λ=1.54178 Å). The surface morphology was investigated using SEM (JEOL Ltd, JSM-6510) at an acceleration voltage of 20 kV. FTIR analysis was performed using a Thermo Fisher Scientific instrument with sample powders diluted in KBr pellets. Photocatalytic degradation of the organic dyes was conducted using a UV-vis spectrophotometer (Perkin-Elmer) in the wavelength range of 200-800 nm with a Lambda 365. The organic dye solution was irradiated with visible light using blue LED (5W, 450 nm, T5 Jinsung Electronic., Ltd).

### 3. Synthesis of nanorod g-$C_3N_4$

Typically, to 100 mL of distilled water, 1.261 g of melamine ($C_3H_6N_6$) and 1.773 g of trithiocyanuric acid ($C_3H_3N_3S_3$) were added, followed by stirring at room temperature for 10 h. The resulting faint yellow precipitation was washed thrice with ethanol by centrifugation. The product was dried at 60°C for overnight, then calcined in an electric furnace at 550°C for 2 h at heating rate of 5°C/min in air atmosphere.

### 4. Synthesis of nanorod g-$C_3N_4$/$Ag_3PO_4$ composites

To synthesize the nanorod g-$C_3N_4$/$Ag_3PO_4$ composite, 0.3 g of the synthesized nanorod g-$C_3N_4$ powder was dispersed in 100 mL of distilled water under ultrasonic irradiation for 60 min. 0.17 g of silver nitrate was dissolved in 20 mL of distilled water. The silver nitrate solution was stirred into the suspended nanorod g-$C_3N_4$ solution using a magnetic stirrer for 30 min.

0.1 M of an aqueous ammonia solution was added dropwise to the solution at room temperature for 50 min. Then, 0.426 g of sodium hydrogen phosphate was dissolved in 15 mL of distilled water, added dropwise and mixed solution was stirred for 30 min. The product was washed thrice with ethanol and dried at 60°C for 12 h.

### 5. Photocatalytic degradation process of organic dyes

The concentration of MB and MO in the organic dye solution was $0.63 \times 10^{-2}$ mM and $3.67 \times 10^{-2}$ mM, respectively. The MB solution exhibited an absorption peak at 665 nm and the MO solution exhibited an absorption peak at 464 nm. The photocatalyst powder (5 mg) was added to a conical tube which containing 10 ml of an aqueous organic dye solution. To achieve adsorption-desorption equilibrium between the organic dye solution and photocatalysts, the conical tubes were kept in the dark environment for 15 min. The blue LED was used to provide a visible light source at a distance of 1 cm between the LED and the aqueous organic dye solution. The photocatalytic degradation of the organic dye was analyzed using a UV-vis spectrophotometer, monitoring at 15 min intervals.

## Results and Discussion

### 1. XRD pattern

Figure 1 shows the XRD pattern of the nanorod g-$C_3N_4$/$Ag_3PO_4$ composites. Peaks at $2\theta = 13.1°$ and 27.6° were owing to the nanorod g-$C_3N_4$ and were assigned to the (100) and (002) planes, respectively. The main peak at $2\theta = 27.6°$ can be indexed to the (002) plane of graphite-like materials (JCPDS card no. 87-1526).[29-31] Peaks at $2\theta = 20.93°$, 29.75°, 33.35°, 36.64°, 42.56°, 47.87°, 52.74°, 55.08°, 57.33°, 61.73°, 66.09°, 69.98°, 71.97°, and 74.24° correspond to the (110), (200), (210), (211), (220), (310), (222), (320), (321), (400), (330), (420), (421), and (332) planes of $Ag_3PO_4$ (JCPDS file No. 06-0505).[32-34] No other diffraction peaks were observed for the nanorod g-$C_3N_4$/$Ag_3PO_4$ composites. The crystallite size of the $Ag_3PO_4$ was calculated using the Scherrer equation[35]:

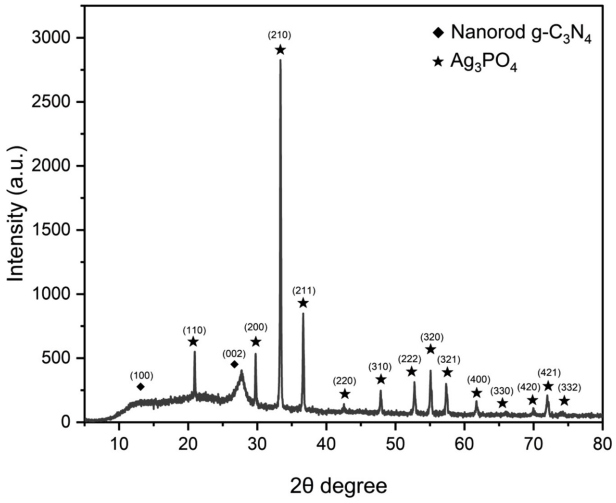


**Figure 1.** XRD pattern of synthesized nanorod g-$C_3N_4$/$Ag_3PO_4$ composites.

**Table 1.** Crystallite size of the $Ag_3PO_4$ in the g-$C_3N_4$/$Ag_3PO_4$ composites.

| (hkl) | 2θ | FWHM | Crystallite size (nm) |
|---|---|---|---|
| (200) | 29.75° | 0.144 | 59.64 |
| (210) | 33.35° | 0.171 | 50.67 |
| (211) | 36.64° | 0.194 | 45.07 |
| Average | | | 51.79 |

$$D = K\lambda / \beta\cos\theta.$$

where D is known as the crystallite size (nm), K is the Scherrer constant taken as 0.9, λ is the wavelength of the X-ray diffraction with Cu Kα, (λ = 1.5418 Å), β is the full width at half maximum (FWHM), and θ is the Bragg angle in degree. Table 1 shows the crystallite size of the $Ag_3PO_4$ at (200), (210), and (211) planes and the mean crystallite size of the $Ag_3PO_4$.

## 2. SEM image

Figure 2 shows the surface morphology of the nanorod g-$C_3N_4$/$Ag_3PO_4$ composites obtained using SEM. The SEM image shows two distinct structural morphologies in the synthesized nanorod g-$C_3N_4$/$Ag_3PO_4$ composites. Nanorod g-$C_3N_4$ exhibited an obvious one-dimensional rod shape, whereas $Ag_3PO_4$ had a cubic shape.

## 3. FT-IR spectra

Figure 3 shows the FTIR spectrum of the nanorod g-$C_3N_4$/

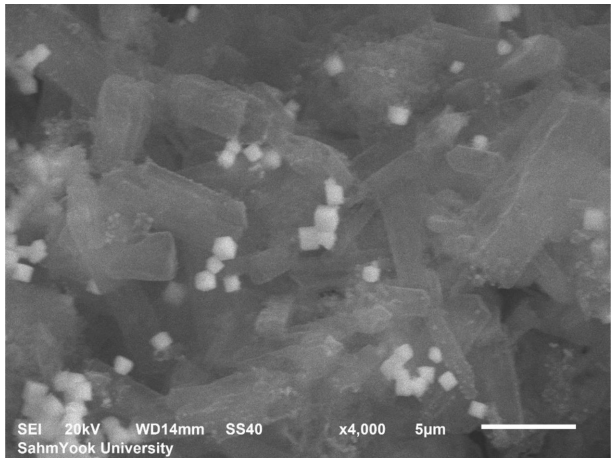


**Figure 2.** SEM image of synthesized nanorod g-$C_3N_4$/$Ag_3PO_4$ composites.

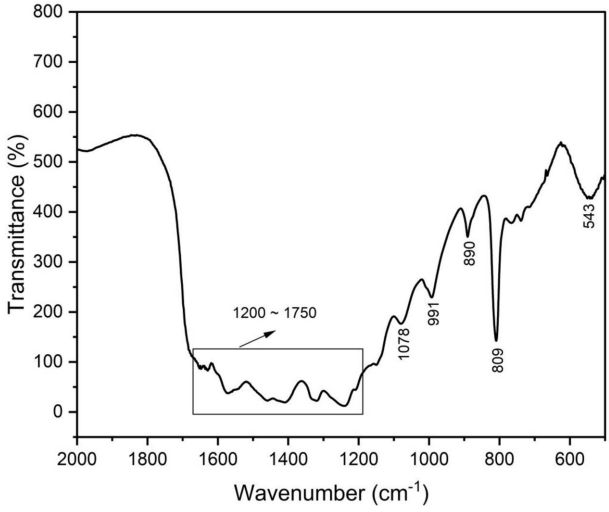


**Figure 3.** FT-IR spectrum of synthesized nanorod g-$C_3N_4$/$Ag_3PO_4$ composites.

$Ag_3PO_4$ composites used to characterize the various functional groups and interactions between the nanorod g-$C_3N_4$ and $Ag_3PO_4$. For nanorod g-$C_3N_4$, the sharp peaks at 809 and 890 $cm^{-1}$ are attributed to the tri-s-triazine unit. The peaks in the range of 1200-1750 $cm^{-1}$ are attributed to the aromatic CN heterocycles. [36-38] For $Ag_3PO_4$, the peaks at 543 $cm^{-1}$ and 991 $cm^{-1}$ are related to the P-O stretching vibration mode of $PO_4^{3-}$. The peak at 1078 $cm^{-1}$ was attributed to the asymmetric stretching vibrations of the P-O-P group.[39-41]

## 4. Photocatalytic degradation efficiency of organic dyes

To study the photocatalytic degradation efficiency (PDE) of organic dyes such as MB and MO, the nanorod g-$C_3N_4$/

$Ag_3PO_4$ composites were irradiated using blue LED at 450 nm. The PDE was calculated using the following equation[42]:

$$PDE(\%) = \frac{C_0 - C_t}{C_0} \times 100 = \frac{I_0 - I_t}{I_0} \times 100$$

where $C_0$ represents the initial concentration of the organic dyes solution and $C_t$ represents the concentration of the organic dyes solution at a certain time $t$. $I_0$ represents the intensity of the maximum absorbance peak in the UV-vis spectrum of the initial organic dye solution and $I_t$ represents the intensity of the maximum absorbance peak in the UV-vis spectrum of the organic dyes solution at a certain time $t$.

Figure 4 shows the UV-vis spectra of photocatalytic degradation of MB and MO. The PDEs of MB and MO under blue LED irradiation were 93.24% and 61.94%, respectively. The photodegradation activity of the nanorod g-$C_3N_4$/$Ag_3PO_4$ composites was higher for MB than MO.

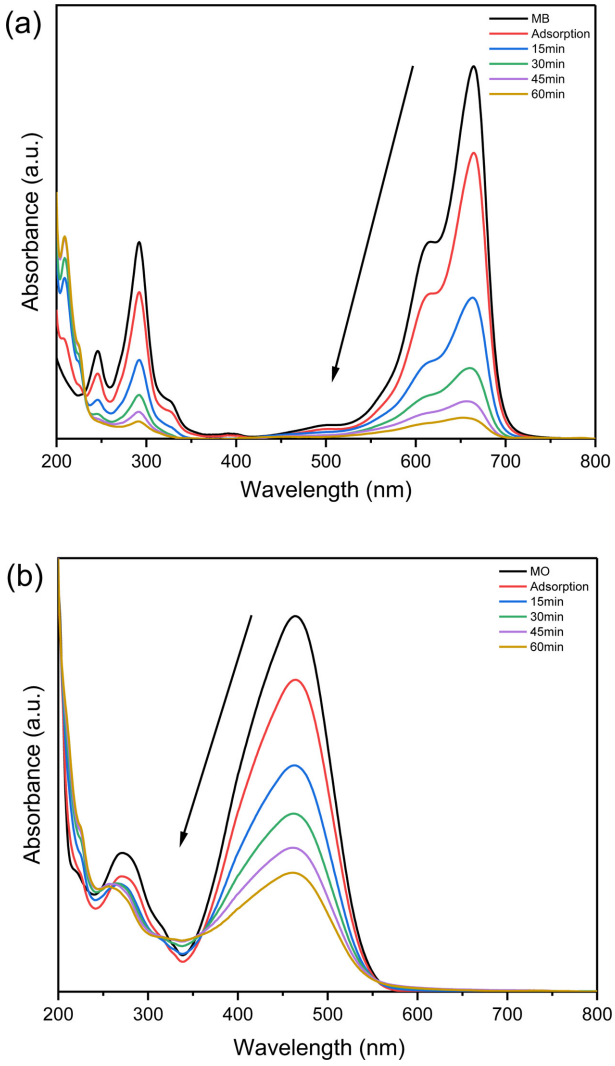


**Figure 4.** UV-vis spectra of photocatalytic degradation of (a) MB and (b) MO using nanorod g-$C_3N_4$/$Ag_3PO_4$ composites under blue LED (450 nm) irradiation.

## 5. Kinetics study

In the Langmuir-Hinshelwood kinetic model, the photocatalytic activity of MB and MO can be represented by the following apparent pseudo-first-order kinetic equations[43]:

$$\ln(C/C_0) = -K \cdot t$$

where $C_0$ represents the initial concentration of the organic dye solution, $C$ represents the concentration at time t, and K is the rate constant of photocatalytic degradation.

MB has cationic properties that allow it to interact with anionic species, such as hydroxyl groups and superoxide anion radicals, on the photocatalytic surface. By contrast, MO tends to react with cationic species such as holes due to its anionic nature.[44] These difference can be attributed to the cationic and anionic properties of organic dye molecules. Figure 5 shows the results of kinetics study for MB and MO. Therefore, the MB had higher photocatalytic degradation efficiency and kinetics rate than for MO.

## 6. Photocatalytic degradation mechanism of organic dyes

Figure 6 illustrates the mechanism of the photocatalytic degradation of organic dyes using nanorod g-$C_3N_4$/$Ag_3PO_4$ composites. Under visible light, photogenerated electrons

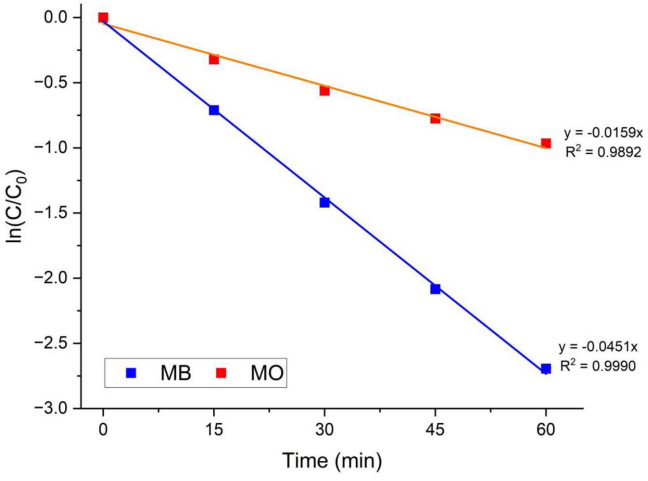


**Figure 5.** Kinetic studies of photocatalytic degradation of MB and MO using nanorod g-$C_3N_4$/$Ag_3PO_4$ composites under blue LED (450 nm) irradiation.

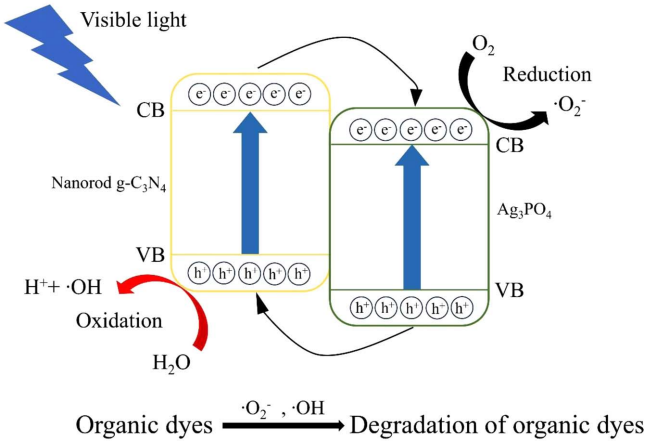


**Figure 6.** Mechanism of photocatalytic degradation for organic dyes using nanorod g-$C_3N_4$/$Ag_3PO_4$ composites under blue LED (450 nm) irradiation.

move from the conduction band of nanorod g-$C_3N_4$ to the $Ag_3PO_4$, while holes move from the valence band of $Ag_3PO_4$ to the nanorod g-$C_3N_4$, showing that the hybrid photocatalysts efficiently separate the photogenerated charges and reduce the recombination of electron-hole pairs. Consequently, water ($H_2O$) is oxidized through the holes ($h^+$) present in the valence band of the nanorods g-$C_3N_4$ to form hydroxyl radical (·OH), while oxygen ($O_2$) is reduced by electrons ($e^-$) from the conducting band of $Ag_3PO_4$ to form superoxide anion radical ($\cdot O_2^-$). The electron and hole pairs can be generated the superoxide anion radicals ($\bullet O_2^-$) and hydroxyl radicals (•OH) species to efficiently degrade organic pollutants.[45,46]

## Conclusions

Rod-like g-$C_3N_4$ was obtained from precursors, such as melamine and trithiocyanuric acid. Nanorod g-$C_3N_4$/$Ag_3PO_4$ composites were synthesized by adding nanorod g-$C_3N_4$ product and silver nitrate ($AgNO_3$), ammonia ($NH_3 \cdot H_2O$ 25.0%-30.0%), and sodium hydrogen phosphate ($Na_2HPO_4$) to distilled water. The nanorod g-$C_3N_4$/$Ag_3PO_4$ composites were characterized using XRD, SEM and FT-IR. The synthesized hybrid photocatalyst was evaluated for the degradation of MB and MO under blue LED irradiation. The photocatalytic degradation processes were observed using a UV-vis spectrophotometer. The degradation of the organic dye process followed pseudo-first-order kinetics. Furthermore, the photocatalytic activity of the nanorod g-$C_3N_4$/$Ag_3PO_4$ composites for MB degradation under visible light was higher than for MO.

## Acknowledgements

This study was supported by Sahmyook University research funding in Korea.

Conflict of Interest: The authors declare that there is no conflict of interest.

## References

1. X. Liu, J. Zhang, Y. Dong, H. Li, Y. Xia, and H. Wang, "A facile approach for the synthesis of Z-scheme photocatalyst ZIF-8/g-$C_3N_4$ with highly enhanced photocatalytic activity under simulated sunlight", *New J. Chem.*, **42**, 12180 (2018).
2. E. Repo, S. Rengaraj, S. Pulkka, E. Castangnoli, S. Suihkonen, M. Sopanen, and M. Sillanpää, "Photocatalytic degradation of dyes by CdS microspheres under near UV and blue LED radiation", *Sep. Purif. Technol.*, **120**, 206 (2013).
3. T. Soltani and M. H. Entezari, "Photolysis and photocatalysis of methylene blue by ferrite bismuth nanoparticles under sunlight irradiation", *J. Mol. Catal. A Chem.*, **377**, 197 (2013).
4. A. Bhatnagar and A. K. Jain, "A comparative adsorption study with different industrial wastes as adsorbents for the removal of cationic dyes from water", *J. Colloid Interface Sci.*, **281**, 49 (2005).
5. R. Guan, J. Li, J. Zhang, D. Wang, H. Zhai, and D. Sun, "Photocatalytic performance and mechanistic research of ZnO/g-$C_3N_4$ on degradation of methyl orange", *ACS Omega*, **4**, 20742 (2019).
6. J. Li, J. W. Ko, and W. B. Ko, "Photocatalytic Degradation of Organic Dyes using CdSe-Mn-$C_{60}$ Nanocomposites", *Elast. Compos.*, **57**, 181 (2022).
7. E. K. Lee and S. Y. Han, "Synthesis and Characterization of the Ag-doped $TiO_2$", *Elast. Compos.*, **57**, 1 (2022).
8. U. Sulaeman, E. Yunari, P. Isanti, S. Yin, and T. Sato, "Synthesis of $Bi_2O_3$/$Ag_3Po_4$ Composites and their Photocatalytic Activities under Visible Light Irradiation", *Adv. Mat. Res.*, **1112**, 163 (2015).
9. C. Song, C. Shang, S. Li, W. Wang, M. Qi, J. Chen, and H. Liu, "Efficient visible-light-responsive $Ag_3PO_4$/g-$C_3N_4$/hydroxyapatite photocatalyst (from oyster Shells) for the degradation of methylene blue: preparation", *Catalysts*, **12**, 115 (2022).
10. W. Zhang, X. Xiao, L. Zheng, and C. Wan, "Fabrication of $TiO_2$/$MoS_2$@zeolite photocatalyst and its photocatalytic

activity for degradation of methyl orange under visible light", *Appl. Surf. Sci.*, **358**, 468 (2015).
11. H. Li, J. Liu, W. Hou, N. Du, R. Zhang, and X. Tao, "Synthesis and characterization of g-$C_3N_4$/$Bi_2MoO_6$ heterojunctions with enhanced visible light photocatalytic activity", *Appl. Catal. B*, **160**, 89 (2014).
12. T. Li, L. Zhao, Y. He, J. Cai, M. Luo, and J. Lin, "Synthesis of g-$C_3N_4$/$SmVO_4$ composite photocatalyst with improved visible light photocatalytic activities in RhB degradation", *Appl. Catal. B*, **129**, 255 (2013).
13. D. Wang, J. Liu, M. Xu, J. Gao, D. Yang, B. Yu, W. Jiang, and H. Li, "Optimized design of visible light-driven g-$C_3N_4$ nanorod/$Ag_3PO_4$ Z-scheme heterojunction with enhanced interfacial charge separation and photocatalytic activity", *J. Mater. Sci. Mater. Electron.*, **33**, 2415 (2022).
14. S. Kumara, S. Ta, A. Baruahb, and V. Shankera, "Synthesis of a novel and stable g-$C_3N_4$-$Ag_3PO_4$ hybrid nanocomposite photocatalyst and study of the photocatalytic activity under visible light irradiation", *J. Mater. Chem. A*, **1**, 5333 (2013).
15. Z. Mo, X. She, Y. Li, L. Liu, L. Huang, Z. Chen, Q. Zhang, H. Xu, and H. Li, "Synthesis of g-$C_3N_4$ at different temperatures for superior visible/UV photocatalytic performance and photoelectrochemical sensing of MB solution", *RSC Adv.*, **5**, 101552 (2015).
16. J. Wen, J. Xie, X. Chen, and X. Li, "A review on g-$C_3N_4$-based photocatalysts", *Appl. Surf. Sci.*, **319**, 72 (2017).
17. X. Wang, K. Maeda, A. Thomas, K. Takanabe, G. Xin, J. M. Carlsson, K. Domen, and M. Antonietti, "A metal-free polymeric photocatalyst for hydrogen production from water under visible light", *Nat. Mater.*, **8**, 76 (2009).
18. B. Fahimirad, A. Asghari, and M. Rajabi, "Magnetic graphitic carbon nitride nanoparticles covalently modified with an ethylenediamine for dispersive solid-phase extraction of lead (II) and cadmium (II) prior to their quantitation by FAAS", *Mikrochim Acta*, **184**, 3027 (2017).
19. P. H. Linh, P. Chung, N. Van Khien, V. T. Thu, T. N. Bach, L. T. Hang, N. M. Hung, and V. D. Lam, "A simple approach for controlling the morphology of g-$C_3N_4$ nanosheets with enhanced photocatalytic properties", *Diam. Relat. Mater.,* **111**, 108214 (2021).
20. W. Touati, M. Karmaoui, A. Bekka, M. F. Edelmannová, C. Furgeaud, A. Chakib, I. K. Allah, B. Figueiredo, J. A. Labrincha, R. Arenal, K. Koci and D. M. Tobaldi, "Photocatalytic hydrogen generation from a methanol–water mixture in the presence of g-$C_3N_4$ and graphene/g-$C_3N_4$", *New J. Chem.* **46**, 20679 (2022).
21. X. Bai, L. Wang, R. Zong, and Y. Zhu, "Photocatalytic activity enhanced via g-$C_3N_4$ nanoplates to nanorods", *J. Phys. Chem.* C, **117**, 9952 (2013).
22. Z. Zhu, W. Fan, Z. Liu, H. Dong, Y. Yan, and P. Huo, "Construction of an attapulgite intercalated mesoporous g-$C_3N_4$ with enhanced photocatalytic activity for antibiotic degradation", *J. Photochem. Photobiol. A*, **359**, 102 (2018).
23. S. Chen, Y. Hu, S. Meng, and Fu. X, "Study on the separation mechanisms of photogenerated electrons and holes for composite photocatalysts g-$C_3N_4$-$WO_3$", *Appl. Catal. B*, **150**, 564 (2014).
24. A. A. Elhakim, M. E. Kemary, M. M. Ibrahim, I. M. El-Mehasseb, and H. S. El-Sheshtawy, "Direct Z-scheme of $WO_3$/GO decorated with silver nanoparticles for synergetic adsorption and photocatalytic activity for organic and inorganic water pollutants removal", *Appl. Surf. Sci.*, **564**, 150410 (2021).
25. L. Liu, Y. Qi, J. Lu, S. Lin, W. An, Y. Liang, and W. Cui, "A stable $Ag_3PO_4$@ g-$C_3N_4$ hybrid core@ shell composite with enhanced visible light photocatalytic degradation", *Appl. Catal. B*, **183**, 133 (2016).
26. H. Zhai, T. Yan, P. Wang, Y. Yu, W. Li, J. You, and B. Huang, "Effect of chemical etching by ammonia solution on the microstructure and photocatalytic activity of $Ag_3PO_4$ photocatalyst", *Appl. Catal. A Gen.*, **528**, 104 (2016).
27. R. Tao, S. Yang, C. Shao, X. Li, X. Li, S. Liu, J. Zhang, and Y. Liu, "Reusable and Flexible g-$C_3N_4$/$Ag_3PO_4$/Polyacrylonitrile Heterojunction Nanofibers for Photocatalytic Dye Degradation and Oxygen Evolution", *ACS Appl. Nano Mater.*, **2**, 3081 (2019).
28. J. J. Liu, X. L. Fu, S. F. Chen, and Y. F. Zhu, "Electronic structure and optical properties of $Ag_3PO_4$ photocatalyst calculated by hybrid density functional method", *Appl. Phys. Lett.*, **99**, 191903 (2011).
29. D. Ayodhya and G. Veerabhadram, "Synthesis and characterization of g-$C_3N_4$ nanosheets decorated $Ag_2S$ composites for investigation of catalytic reduction of 4-nitrophenol, antioxidant and antimicrobial activities", *J. Mol. Struct.*, **1186**, 423 (2019).
30. F. Fina, S. K. Callear, G. M. Carins, and J. T. Irvine, "Structural investigation of graphitic carbon nitride via XRD and neutron diffraction", *Chem. Mater.*, **27**, 2612 (2015).
31. Y. Guo, L. Xiao, M. Zhang, Q. Li, and J. Yang "An oxygen-vacancy-rich Z-scheme g-$C_3N_4$/Pd/$TiO_2$ heterostructure for enhanced visible light photocatalytic performance", *Appl. Surf. Sci.*, **440**, 432 (2018).
32. A. Amedlous, M. Majdoub, E. Amaterz, Z. Anfar, and A. Benlhachemi, "Synergistic effect of g-$C_3N_4$ nanosheets/$Ag_3PO_4$ microcubes as efficient n-p-type heterostructure based photoanode for photoelectrocatalytic dye degradation", *J. Photochem. Photobiol. A*, **409**, 113127 (2021).
33. Y. Song, Y. Lei, H. Xu, C. Wang, J. Yan, H. Zhao, Y. Xu, J.

Xia, S. Yin, and H. Li, "Synthesis of few-layer $MoS_2$ nanosheet-loaded $Ag_3PO_4$ for enhanced photocatalytic activity", *Dalton Trans*., **44**, 3057 (2015).
34. W. Teng, X. Tan, X. Li, and Y. Tang, "Novel $Ag_3PO_4$/$MoO_3$ p-n heterojunction with enhanced photocatalytic activity and stability under visible light irradiation", *Appl. Surf. Sci.*, **409**, 250 (2017).
35. M. E. Taheri, A. Petala, Z. Frontistis, D. Mantzavinos, and D. I. Kondarides, "Fast photocatalytic degradation of bisphenol A by $Ag_3PO_4$/$TiO_2$ composites under solar radiation" *Catal. Today*, **280**, 99 (2017).
36. X. Wang, J. Song, Y. Lu, W. Zhu, and G. Hu, "Development of a Z-scheme Ag/$Ag_2WO_4$/g-$C_3N_4$ photocatalyst for RhB fast degradation assisted with $H_2O_2$", *J. Mater. Sci. Mater. Electron.*, **32**, 2061 (2021).
37. W. Wang, Q. Niu, G. Zeng, C. Zhang, D. Huang, B. Shao, C. Zhou, Y. Yang, Y. Liu, H. Guo, W. Xiong, L. Lei, S. Liu, H. Yi, S. Chen, and X. Tang, "1D porous tubular g-$C_3N_4$ capture black phosphorus quantum dots as 1D/0D metal-free photocatalysts for oxytetracycline hydrochloride degradation and hexavalent chromium reduction", *Appl. Catal.*, **273**, 119051 (2020).
38. B. Zhu, P. Xia, Y. Li, W. Ho, and J. Yu, "Fabrication and photocatalytic activity enhanced mechanism of direct Z-scheme g-$C_3N_4$/$Ag_2WO_4$ photocatalyst", *Appl. Surf. Sci.*, **391**, 175 (2017).
39. W. Zhang, L. Zhou, J. Shi, and H. Deng, "Synthesis of $Ag_3PO_4$/G-$C_3N_4$ composite with enhanced photocatalytic performance for the photodegradation of diclofenac under visible light irradiation", *Catalysts*, **8**, 45 (2018).
40. Q. Liang, W. Ma, Y. Shi, Z. Li, and X. Yang, "Hierarchical $Ag_3PO_4$ porous microcubes with enhanced photocatalytic properties synthesized with the assistance of trisodium citrate", *CrystEngComm*, **14**, 2966 (2012).
41. R. K. Santos, T. A. Martins, G. N. Silva, M. V. Conceição, I. C. Nogueira, E. Longo, and G. Botelho, "$Ag_3PO_4$/NiO composites with enhanced photocatalytic activity under visible light", *ACS Omega*, **5**, 21651 (2020).
42. V. A. Tran, T. P. Nguyen, I. T. Kim, S.-W. Lee, and C. T. Nguyen, "Excellent photocatalytic activity of ternary Ag@$WO_3$@rGO nanocomposites under solar simulation irradiation", *J. Sci.: Adv. Mater. Devices*, **6**, 108 (2021).
43. K. Dai, L. Lu, C. Liang, Q. Liu, and G. Zhu, "Heterojunction of facet coupled g-$C_3N_4$/surface-fluorinated $TiO_2$ nanosheets for organic pollutants degradation under visible LED light irradiation", *Appl. Catal. B*, **156**, 331 (2014).
44. A. Dana and S. Sheibani, "CNTs-copper oxide nanocomposite photocatalyst with high visible light degradation efficiency", *Adv. Powder Technol.*, **32**, 3760 (2021).
45. P. He, L. Song, S. Zhang, X. Wu, and Q. Wei, "Synthesis of g-$C_3N_4$/$Ag_3PO_4$ heterojunction with enhanced photocatalytic performance", *Mater. Res. Bull.*, **51**, 432 (2014).
46. D. Jiang, J. Zhu, M. Chen, and J. Xie, "Highly efficient heterojunction photocatalyst based on nanoporous g-$C_3N_4$ sheets modified by $Ag_3PO_4$ nanoparticles: Synthesis and enhanced photocatalytic activity", *J. Colloid Interface Sci.*, **417**, 115 (2014).